

Locking of electrostatically coupled thermo-optically driven MEMS limit cycle oscillators

Alan T. Zehnder ^{a,*}, Richard H. Rand ^a, Slava Krylov ^b

^a Field of Theoretical and Applied Mechanics, Sibley School of Mechanical and Aerospace Engineering, Cornell University, Ithaca NY 14853, United States

^b School of Mechanical Engineering, Faculty of Engineering, Tel Aviv University, Ramat Aviv 69978 Tel Aviv, Israel



ARTICLE INFO

Keywords:

Micro-electro mechanical systems
Limit cycle oscillator
Phase locking
Numerical analysis
Parametric excitation

ABSTRACT

A model of coupled limit cycle oscillators is developed and analyzed to discover and map out the system's locking behavior. This sixth order model is motivated by the physical problem of a pair of closely spaced doubly clamped, thin silicon beams, coupled to each other through electrostatic fringing fields. The beams are assumed to be detuned with respect to each other. The beams are optically thin and are situated above a thick silicon substrate. When illuminated with continuous laser light a cavity interferometer is formed. Coupling of this optical interference with thermal stresses creates an inherent feedback loop that can drive the beams into limit cycle oscillation. Numerical analysis is used to study the range of coupling strengths and detunings over which 1:1, and other integer frequency ratio locking can be obtained. Results show that 1:1 locking can occur over a broad range of detuning even at relatively low levels of coupling. For coupling strengths just above the threshold for locking, both locked and drift states can exist, depending on the initial conditions. Locking at 2:1, 3:1, 3:2 and 5:2 frequency ratios are observed for detunings that are close but not exactly equal to these integer ratios.

1. Introduction

Micro- and nano-electromechanical systems (MEMS and NEMS) have revolutionized applications such as sensing [1–3], navigation [4,5], signal processing [6,7], ink jet printing [8] and optical switching [9]. Many of the MEMS sensors exploit linear and nonlinear resonance behavior [10,11] in which the dependence of a dynamical response such as frequency and phase on physical characteristics such as mass absorption or acceleration [12] is used to transduce the desired quantity. Such devices typically consist of small scale, flexible structures with dimensions in the micron to nanometer range. Although this technology has advanced rapidly, the space for design of transformative MEMS and NEMS is still wide open. One of the keys to exploiting this design space is the discovery and understanding of non-linear dynamic phenomena in MEMS and NEMS.

An example of the importance of nonlinearity in MEMS resonant sensors is found in Ref. [13]. In this experiment a cantilever beam is coated with a polypyrrole receptor layer which swells as it adsorbs ethanol, producing a static bending and a shift in frequency. By operating the system at high amplitude and near jumps in the amplitude–frequency response (backbone curve) the frequency change due to adsorption was enhanced by about 3× relative to operation in the linear regime, showing a path to high sensitivity chemical sensors.

While future systems may exploit large arrays of oscillators, the focus here is on a model for the nonlinear dynamics of a pair of coupled, thermo-optical limit cycle oscillators (LCO). In the envisioned system a thermo-optical feedback mechanism induces limit cycle oscillations in flexible micro-scale beams. A static voltage difference between the beams couples the oscillators through forces caused by electro-static fringing fields [14]. As a prelude to design, fabrication and testing of such systems, a model is developed here and investigated to determine the coupling strength needed for 1:1 frequency ratio locking of two opto-thermal LCOs with different individual frequencies. The analysis also explores the frequency to which the LCOs lock, the effect of the strength of the cubic nonlinearity on locking, the effect of initial conditions on locking for weak coupling strengths and the regions of 2:1, 3:1, 3:2 and 5:2 frequency ratio locking.

The literature on coupled LCOs provides insights into the phenomena that are likely to occur in the envisioned, current system. A simple analog to the system studied here is two linearly coupled, detuned van der Pol oscillators [15–17]. As the coupling strength is increased, the system will transition from drift in which the relative phases of the two oscillators diverge, to a weakly locked (or phase entrained) mode in which the phase difference varies periodically with zero average, to strongly locked (or phase locked) in which the phase difference is zero.

* Corresponding author.

E-mail addresses: atz2@cornell.edu (A.T. Zehnder), vadis@eng.tau.ac.il (S. Krylov).

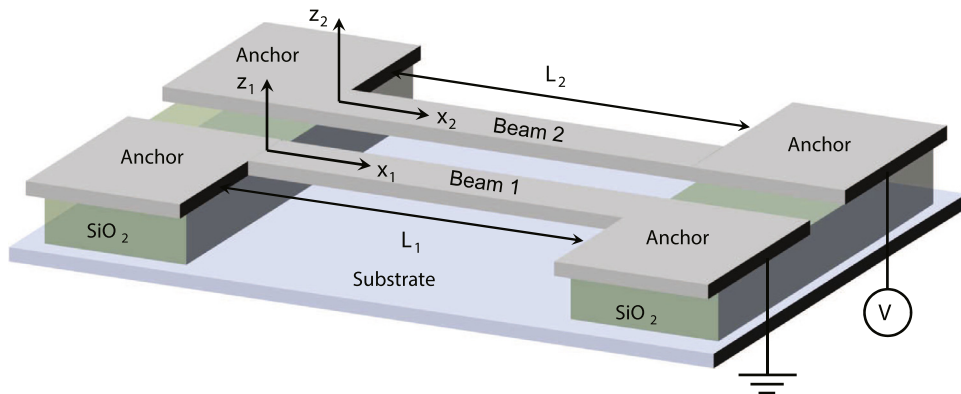


Fig. 1. Two doubly clamped nano-beams with electrostatic coupling.

Locking can be in- or out-of-phase [18]. Note that many authors refer to locking of oscillators, as described above, as frequency locking [19] or synchronization [20–22]. Locking of an oscillator to an external signal (not studied here) is often referred to as entrainment [23,24] or injection locking [25] or simply as locking [26]. In this paper we use “locking” to refer to synchronization of oscillators at 1:1 or M:N frequency ratios, where M and N are integers. In all cases studied here the 1:1 locking is “weak” meaning that the phase difference varies periodically, but with a constant average.

Several groups have explored MEMS resonators coupled through electrostatic attraction. A low frequency vibration sensing system was developed by coupling a highly damped low frequency resonator to a high Q (low damping), high frequency resonator [27,28]. The mixing of these signals transforms the vibration signal into a high frequency signal that is then measured to infer the amplitude and frequency of sensed, low frequency vibration. A pair of cantilever based oscillators with feedback proportional to the sum of their velocities was shown to lock when the pair’s uncoupled frequencies are within the 3 dB bandwidth and to oscillate separately (drift) when the frequency difference is greater than this threshold [29]. Two plate shaped resonators set into LCO via displacement feedback were observed to oscillate with reduced phase noise relative to the individual oscillators [30]. Similarly, two electrostatically coupled oscillators were seen to lock with in- or out-of-phase motion [31]. Analytical models of the system predict very similar results. Locking of thermally driven dome shaped oscillators is studied in Ref. [32]. Under one-way coupling in which oscillator 1 sees a heater voltage proportional to the displacement of oscillator 2, the LCOs lock with a relative phase that depends on the sign of the coupling coefficient. Two capacitively coupled oscillators with hardening behavior are observed to improve their frequency stability by 7× when phase locked, [33] an important result for applications such as MEMS based clocks. Pairs of coupled, piezoelectrically actuated beams were studied experimentally and numerically in Ref. [20]. Similar to [33] relative to the unlocked case, a reduction in phase noise of -3 dB was observed when the oscillators locked. Partial and complete injection locking of two coupled modes of a doubly clamped SiNi beam to a common parametric drive was experimentally demonstrated in Ref. [25].

A description of the physical system under investigation is provided in the next section, followed by the model and a discussion of the system parameters. The behavior of a single LCO is described to set the stage for analysis and discussion of 1:1, 2:1, 3:1, 3:2 and 5:2 locking of two detuned LCOs. At low coupling strengths the locking regions are dependent on the initial conditions. At the lock/drift boundary of the 1:1 coupled state an unstable out-of-phase mode is found.

2. Physical system

A system of two, electrostatically coupled limit cycle oscillators, as sketched in Fig. 1, motivates the model analyzed here. Physically

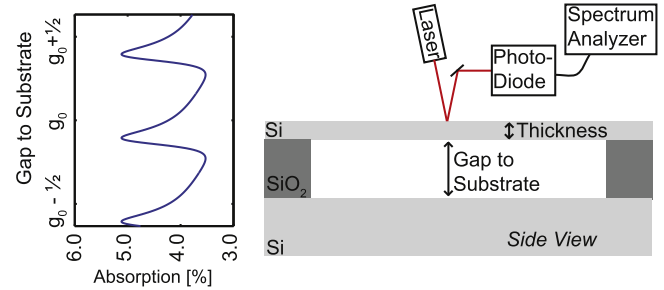


Fig. 2. Schematic setup. The absorbed and reflected laser power are periodic with the gap between the beam and substrate. Inset plots the fraction of laser power absorbed vs. the gap for an optically thin Si beam above a gap. The inherent coupling of absorbed light and the resulting heating to motion can induce limit cycle oscillation.

such a system would consist of two micron size scale, doubly clamped beams fabricated from a device layer of a silicon on insulator (SOI) wafer. Each beam is attached to two anchors and is designed to deflect in the out-of-plane (z) direction. Deliberately, or via variations in the fabrication process, the two beams will have different dimensions leading to different linear (i.e. low amplitude) and LCO frequencies. The two beams are fabricated with a small gap between them. A voltage difference is applied between the beams. The resulting fringing electrostatic field [14] couples the beams through a force that is linear for small differences in beam deflection but drops off as the difference increases.

The setup for inducing opto-thermal LCOs in a single micro-scale beam resonator is outlined in Fig. 2. The Si resonator is optically thin (can transmit light) and is suspended over a thick substrate. A continuous laser is focused to a spot at the center of the resonator. In typical experiments the resonator is mounted in a high vacuum system to eliminate viscous damping. Laser light incident on the resonator is partially absorbed, partially reflected and partially transmitted. Transmitted light is reflected from the substrate back to the resonator. The net result is that the resonator-gap-substrate system forms a Fabry-Pérot cavity interferometer whose laser absorption and reflection depend on the gap. As the resonator moves through the interference field, it modulates the reflected and absorbed light and hence the thermal stress in the beam. Thermal stress induces vertical deflection of the beam. Deflection modulates the absorbed light and hence the temperature, leading to a feedback loop that can drive limit cycle oscillations. This general setup has been used to excite and study oscillations in resonators of various sizes and shapes including cantilevers, doubly clamped beams, disks, and domes [34,35].

Table 1

Parameter values used in analysis [35]. The electrostatic parameter p is estimated from Ref. [38].

Parameter	Value	Units
H	6780	K/W
B	.112	
α	0.035	
γ	0.011	
z_0	0.18	
C	.02	1/K
D	2.84×10^{-3}	1/K
Q	1240	
β	15.5	
p	2.4	

3. Model of system

The mathematical model extends the model of a single, thermo-optically driven MEMS oscillator [34,36,37] to a pair of such oscillators coupled by electrostatic fringing fields. With time normalized to the small amplitude period of oscillation, and the displacements z_1 and z_2 of the first modes of oscillators 1 and 2 normalized by the laser wavelength, a simplified model capturing the absorption of light, its modulation due to motion, the effect of temperature on the mechanics and the electrostatic coupling is:

$$\ddot{z}_1 + \frac{\dot{z}_1}{Q} + (1 + CT_1)z_1 + \beta z_1^3 + \frac{V^2(z_1 - z_2)}{1 + |z_1 - z_2|^p} = DT_1, \quad (1)$$

$$\dot{T}_1 = -BT_1 + HP_{laser}[\alpha + \gamma \sin^2(2\pi(z_1 - z_0))], \quad (2)$$

$$\ddot{z}_2 + \frac{\dot{z}_2}{Q} + \kappa(1 + CT_2)z_2 + \beta z_2^3 + \frac{V^2(z_2 - z_1)}{1 + |z_2 - z_1|^p} = DT_2, \quad (3)$$

$$\dot{T}_2 = -BT_2 + HP_{laser}[\alpha + \gamma \sin^2(2\pi(z_2 - z_0))]. \quad (4)$$

The mechanical model is similar to a Mathieu–Duffing resonator with forcing proportional to temperature. The Mathieu type term, $(1 + CT)z$, provides parametric excitation at twice the oscillator's frequency through the thermal coupling. The Duffing term, βz^3 leads to amplitude dependent frequency, which will be one of the keys to locking. The thermal model is reduced to a lumped thermal mass with laser heating and Newton's law of cooling. All quantities in the above are non-dimensional with the exception of temperature, T , given in K and laser power, P_{laser} , given in W. In the thermal equations, T_1 and T_2 are the average temperatures of oscillators 1 and 2, B and H are thermal constants, P_{laser} is the laser power, α is the minimum absorption, γ is the contrast in absorption, and z_0 represents the equilibrium position of the oscillator with respect to the absorption curve. In the mechanical equations Q is the quality factor, β is the cubic stiffness, C is a coefficient relating linear stiffness change to temperature and D is the static displacement per unit temperature change. The form of the electrostatic coupling (V^2 term) is approximated from Ref. [38,39]. The voltage parameter, V^2 can be considered as inclusive of the actual voltage squared multiplied by a coupling coefficient, that for an actual device would be determined by finite element analysis [38,39]. The natural frequencies of neighboring MEMS oscillators will be close, but not exactly the same due to fabrication variations. Thus, in the model, the linear frequency of oscillator 2 is detuned from oscillator 1 by the ratio $\sqrt{\kappa}$. The fixed model parameters are taken from Ref. [35] and are given in Table 1. In experiments the value of Q has been observed to be as high as 10,000, however a smaller value, $Q = 1240$, (higher damping) was taken in order to speed up the time for the solution to reach steady state oscillation. The main effect of lower Q is that laser power, P_{laser} , needed to induce limit cycle motion will increase; it scales linearly with $1/Q$ [34].

To start to understand the behavior of this system and the space in which locking will occur, the above system has been integrated numerically and the results interrogated to determine the system behavior

over a range of locking strengths, detuning ratios and initial conditions. The analysis below will show that the system may have a number of responses, including: 1:1 in-phase “weak locking” in which the two LCOs have the same frequency and a constant, average phase difference or “drift” in which the two LCOs run at their separate frequencies. An unstable out-of-phase 1:1 locking mode is found to exist at the lock/drift boundary in the space of initial conditions. Integer frequency ratio (2:1, 3:1, 3:2 and 5:2) phase locking regions are found using a model modified to account for large detunings.

3.1. Analysis method

The system of equations above is converted to six coupled first order equations in the variables $(z_1, \dot{z}_1, T_1, z_2, \dot{z}_2, T_2)$ and numerically integrated using a Python code. The Python (SciPy) ordinary differential equation solver, “odeint” uses the LSODA routine from the FORTRAN library ODEPACK [40]. Small jobs were run on a desktop computer, while runs involving sweeping over a large parameter set were performed in parallel on a multi-core computer. Parameters swept over include laser power, P_{laser} , detuning, κ , and the electrostatic coupling voltage, V . For each parameter set the computations were run to a time span of $20Q$ or more to ensure that steady state oscillations were achieved. As an estimate of the computing cost, a sweep over 12500 parameter pairs required approximately 38 core-hours.

To determine if the oscillators are locked, the Hilbert transforms [41] of the steady state $z_1(t)$ and $z_2(t)$ were computed. From the Hilbert transform the phase $\phi_1(t)$ and $\phi_2(t)$ of each oscillator was calculated up to an arbitrary constant and the frequencies, ω_1 and ω_2 obtained as the time averages of ϕ_1 and ϕ_2 . If the difference between these frequencies was within 0.001 the oscillators are considered to be locked. The instantaneous phase difference, $\Delta\phi(t) = \phi_1(t) - \phi_2(t)$ was also computed. If $\Delta\phi(t)$ is constant then strong locking would occur. If $\Delta\phi(t)$ is periodic with a constant average then weak locking occurs. If $\Delta\phi(t)$ increases with time then the system drifts. The above method yields only the fundamental frequency, thus to examine the frequency content of $z_1(t)$ and $z_2(t)$, the FFTs of the steady state results were also computed.

4. Behavior of a single LCO

We start with an analysis of the dynamics of a single thermo-optical limit cycle oscillator [34,35]. Setting $V = 0$, and sweeping the laser power, P_{laser} , up and down, the system of Eqs. (1) and (2) is integrated until steady state is reached, starting from initial conditions $(z_1 = 0, \dot{z}_1 = 0, T_1 = 0)$. The values of (z_1, \dot{z}_1, T_1) at the end of the integration are used as the initial conditions for the next P_{laser} value.

The resulting amplitude and frequency of oscillation are shown in Figs. 3 and 4. As P_{laser} is increased from zero, a supercritical Hopf bifurcation occurs at $P_{laser} = P_{Hopf} \approx 0.0008$ W. The value of P_{Hopf} depends on $1/Q$ as well as other system parameters, [34]. The bifurcation can be sub- or super-critical, depending most strongly on z_0 [34,35]. Fig. 4 shows that as the laser power, and hence the amplitude of motion increase, the frequency of oscillation increases as would be expected for a Duffing oscillator [42].

A key to the ability of the two LCOs to lock is the frequency tunability resulting from the relatively large cubic stiffness nonlinearity, the βz_1^3 and βz_2^3 terms in Eqs. (1) and (3). Figs. 3 and 4 show that there is a unique relationship between laser power, amplitude and frequency. However as will be shown below, for the case of coupled oscillators at a fixed P_{laser} , the amplitude and frequency of the LCO can move up or down the backbone curve, see Fig. 4, as needed to accommodate locking. Similar behavior was found in the analysis of a single LCO entrained to an inertial drive [23]. In that case, for inertial drive frequencies that lead to entrainment the LCO amplitude and frequency moved along the backbone curve as the frequency of the inertial signal was swept.

In all analyses that follow P_{laser} will be fixed at 0.002 W, well above P_{Hopf} . At this P_{laser} value, when the oscillators are uncoupled ($V^2 = 0$) the frequency of LCO 1 is $\omega_1 = 1.173$ with an amplitude of 0.155.

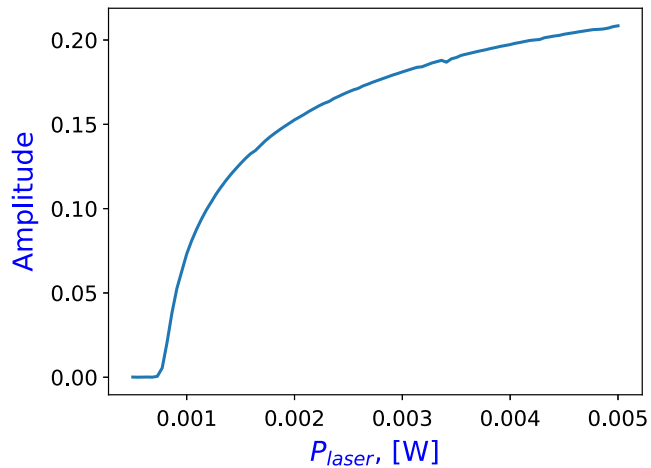


Fig. 3. Normalized amplitude of a single LCO vs. laser power. Hopf bifurcation occurs at $P_{laser} = 0.0008$ W.

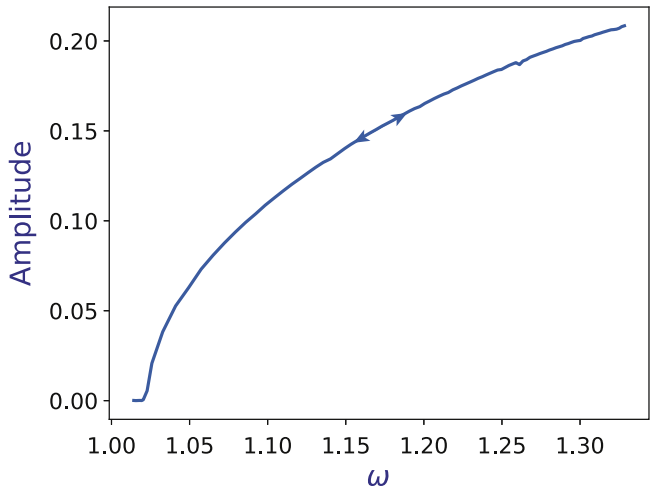


Fig. 4. Normalized amplitude–frequency relationship for a single LCO. The arrows indicate that the frequency can be tuned by changing the amplitude of the LCO.

5. 1:1 locking

5.1. Locking in space of detuning ratio $\sqrt{\kappa}$ and coupling strength V^2

The key question addressed in this analysis is: what level of electrostatic coupling would be needed to lock two oscillators whose uncoupled frequencies differ from each other? The frequency differences could arise from limitations on the fabrication precision or could be intentional. LCO 1 has a linear frequency of one. LCO 2 has a linear frequency of $\sqrt{\kappa}$. When $\kappa = 1$ the LCOs are identical. All system parameters except κ and V^2 are held constant. The results below will show that for low coupling strengths some initial conditions will lead to 1:1 frequency ratio weak locking behavior while other initial conditions will lead to drift. The most experimentally relevant set of initial conditions is that all quantities start at zero, thus in the following, the integrations are performed with all initial conditions set to zero.

Consider first the uncoupled case, $V^2 = 0$, varying $\sqrt{\kappa}$ from 0.6 to 1.3. As Fig. 5 shows $\omega_1 = 1.173$ is constant and ω_2 increases with $\sqrt{\kappa}$. Note that the presence of the cubic nonlinearity, βz_2^3 in Eq. (3) means that the LCO frequency is amplitude dependent and is not linear with $\sqrt{\kappa}$.

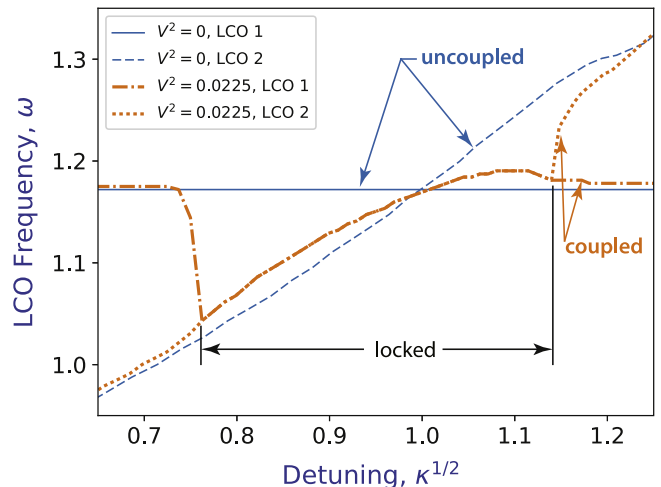


Fig. 5. LCO frequencies vs. detuning for uncoupled and coupled cases.

If V^2 is set to $V^2 = 0.0225$ the LCOs are coupled and, as Fig. 5 shows, will lock for $0.76 < \sqrt{\kappa} < 1.14$. For $\sqrt{\kappa} < 1$ the frequency of the locked pair is pulled down close to the uncoupled frequency of LCO 2. For $\sqrt{\kappa} > 1$ the frequency of the locked pair is pulled down close to the uncoupled frequency of LCO 1. Thus the frequency of the locked system is always close to the lower of the uncoupled frequency of LCO 1 or LCO 2. This is in contrast to phase only models in which the lock frequency is the average of the unlocked LCO frequencies [42]. Analysis of the phase difference, $\Delta\phi(t)$, shows that the oscillators are weakly locked. That is, the average of the phase difference is constant, but periodic with a period that matches that of the locked LCOs. As the coupling strength is increased the amplitude of the periodic oscillation of the phase difference is reduced but never eliminated.

To complete the picture of locking a set of analyses was performed sweeping over the detuning ratio, $\sqrt{\kappa}$ and V^2 . Each integration starts at zero initial conditions. The results are shown in Fig. 6(a) and the zoomed in view at low coupling strengths, Fig. 6(b). A point is plotted if the LCOs lock according the criterion $|\omega_1 - \omega_2| \leq 0.001$.

As would be expected based on the analysis of coupled van der Pol oscillators [17], as coupling strength increases, the range of detuning over which oscillators lock increases. What was unexpected is that the lower bound of the locking space is almost flat, thus the coupling strength needed for locking is nearly constant for $0.9 < \sqrt{\kappa} < 1.05$. This is in contrast to analysis of coupled van der Pol models that show that the coupling strength needed for 1:1 locking is linear in the detuning [18]. A second unexpected result is the erosion of the lower locking boundary, namely the existence of gaps in the locking space for $V^2 < 0.004$, near the lock/drift boundary. The reason for this erosion is explored in the section below on sensitivity to initial conditions.

5.2. Effect of cubic nonlinearity

The ability of the LCOs to lock over a wide range of detuning arises from the large tunability of each individual oscillator due to the cubic stiffness nonlinearity, represented by the βz_1^3 and βz_2^3 terms in Eqs. (1) and (3). As Fig. 4 shows the LCO frequency can vary up to about 30% over the plotted amplitude range. Fig. 5 shows that as detuning is swept, the faster of the two LCOs slows down to approximately the frequency of the slower LCO. If β is reduced then the tunability of each LCO is reduced and it is expected that the locking region will narrow. This is confirmed by the results shown in Fig. 6(a) where the boundaries of the lock region for lower values of β , ($\beta = 10$ and 5) are superimposed on the results for $\beta = 15.5$.

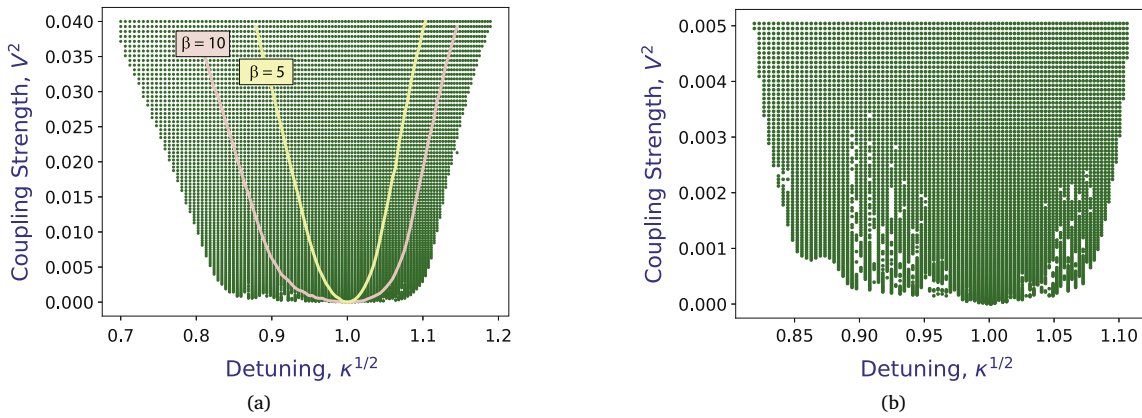


Fig. 6. (a) Locking of LCOs 1 and 2 as a function of the detuning ratio, $\sqrt{\kappa}$ and coupling strength, V^2 . Initial conditions are $z_1(0) = z_2(0) = 0$. Also shown are the boundaries of the locking region for lower values of cubic stiffness nonlinearity, $\beta = 5$ and $\beta = 10$. (b) Detail of locking region for small values of coupling, V^2 .

5.3. Sensitivity to initial conditions

As Fig. 6(b) shows, at low coupling strengths the boundary of the locking space is not smooth and there are holes in the space. Analyses of other coupled oscillator systems shows that locking is sensitive to initial conditions. In studies of coupled metronomes [43] and pendulums [44] it was found that the systems can lock to either in-phase or to out-of-phase modes depending on the initial conditions. The size of the basin of attraction, i.e. the size of the regions in initial condition space that lead to locking was found to depend on coupling strength and connectivity for systems consisting of a large number of oscillators [45]. In a study of coupled, piezoelectrically driven beams it was found that near the boundaries of the coupling space the fraction of randomly generated initial conditions that lead to locking transitions from zero to one as the coupling strength is increased [20].

The observation of holes in Fig. 6(b) and the results of the above prior studies led to the question: Can locked and drift states co-exist? To explore this question a series of analyses were performed varying the coupling strength, V^2 , holding $\sqrt{\kappa} = 0.90$, holding the initial conditions $\dot{z}_1(0) = \dot{z}_2(0) = T_1(0) = T_2(0) = 0$ and varying the initial conditions $(z_1(0), z_2(0))$ over a grid of ± 0.4 .

Results of this analysis are shown in Fig. 7. As the coupling strength increases to $V^2 \geq 0.013$ the LCOs will lock for any initial conditions. However, at low coupling strengths, for example $V^2 = 0.010$ the LCOs lock inside two wedge-like regions given approximately by $z_2(0) \geq |z_1(0)|$ and $z_2(0) \leq -|z_1(0)|$. As V^2 is further reduced only a skeletal region of coupling is found in the initial condition space. These results show that near the threshold of locking the system may either lock or drift depending on initial conditions. If $\sqrt{\kappa} > 1$ then the orientation of the wedge-like region of locking is rotated by 90° in the space of $(z_1(0), z_2(0))$. The lock and drift states can be said to be locally stable for $V^2 < 0.013$ and the lock state to be stable for $V^2 \geq 0.013$.

To further explore the lock vs. drift behavior and to verify that the results of Fig. 7 are correct, a series of integrations were performed for initial conditions at the lock/drift boundary. With all other initial conditions set to zero, setting the coupling below the value at which all IC lead to locking, $V^2 = 0.010$, $\sqrt{\kappa} = 0.90$, $z_2(0) = 0.25$ and iterating $z_1(0)$ it was found that $z_1(0) = 0.2667592$ lies very near the lock/drift boundary. Note that for $\sqrt{\kappa} = 0.90$ if the LCOs are uncoupled they will have frequencies of $\omega_1 = 1.173$ and $\omega_2 = 1.107$ with amplitudes of 0.155 and 0.170 respectively.

For a point just to the left of the lock/drift boundary, $z_1(0) = 0.2667590$ and $V^2 = 0.010$ the LCOs are found to lock in-phase at a frequency of 1.131. Fig. 8(a) shows that when locked the two LCOs have identical phase and frequency. Since the frequency of LCO 1 is pulled down relative to its uncoupled value (see Fig. 5), its amplitude is also reduced. Similarly the amplitude of LCO 2 is increased relative to its

uncoupled value. The FFTs of z_1 and z_2 are shown in Fig. 8(b). Peaks in the FFT are seen at the fundamental frequency of 1.131 and at $2\times$ and $3\times$ multiples of the fundamental frequency. The $3\times$ peak arises from the cubic stiffness nonlinearity, while the $2\times$ peak arises from the \sin^2 term in the thermal equations. The strong $2\times$ and $3\times$ peaks suggest that fairly robust 2:1 and 3:1 locking regions should occur in this system.

Changing the initial condition $z_1(0)$ by $+0.000001$ to $z_1(0) = 0.2667600$, the system was found to drift. Fig. 9(a) shows that the LCOs have different frequencies and that the phase is drifting. The FFTs, Fig. 9(b) show peaks at $\omega_1 = 1.168$ for LCO 1 and $\omega_2 = 1.117$ for LCO 2. Although they are not locked, due to the coupling, the two LCOs still have an effect on each other as seen by the multiple side bands in the FFTs of z_1 and z_2 and by the difference in the LCO frequencies relative to the corresponding uncoupled case.

The results show that in the space of initial conditions there is a boundary between in-phase locking and drift. This leads to the question of what is the nature of the system response on this boundary? Since the lock and drift states are both locally stable, an unstable response must exist on the boundary. Looking at the short time response of the system with $z_1(0) = 0.2667600$ and $z_2(0) = 0.25$ Fig. 10 shows that starting from an approximately in-phase set of initial conditions, the system quickly reaches an out-of-phase 1:1 lock with a frequency of 1.298 and a steady phase difference of π . However, this out-of-phase state is unstable and after $t = 250$ (about 40 cycles) the phase diverges from π as the solution evolves to the locally stable drift state. For a slightly lower value, just inside the lock region, $z_1(0) = 0.2667592$, the system quickly reaches out-of-phase 1:1 lock but then evolves to the 1:1 in-phase lock state. Thus on the boundary the system can for a short time be in the out-of-phase lock, but will evolve either to drift or in-phase lock depending on which side of the boundary the initial condition is.

To provide a more complete picture of the dependence of locking on initial conditions a set of analyses were performed using initial conditions $(\dot{z}_1(0) = \dot{z}_2(0) = T_1(0) = T_2(0) = 0)$. Random values of $z_1(0)$ and $z_2(0)$ were generated over the space $0 \leq z_1(0) \leq 0.4$, $0 \leq z_2(0) \leq 0.4$. The calculation was repeated 25 times and the fraction of initial conditions that led to locking calculated. The results are shown in Fig. 11. An inner region where all initial conditions lead to locking is surrounded by a region in which lock and drift states coexist.

6. Integer ratio locking

Phase only models, derived from perturbation analysis of coupled van der Pol oscillators, show that locking can occur at 1:1, 2:1 and other integer frequency ratios [46]. For example in [46] the region of parameter space lying between 1:1 and 2:1 locking is described as including a region of 3:2 locking as well as smaller regions of M:N locking, where the ratio M/N lies between 1 and 2. In a study of coupled

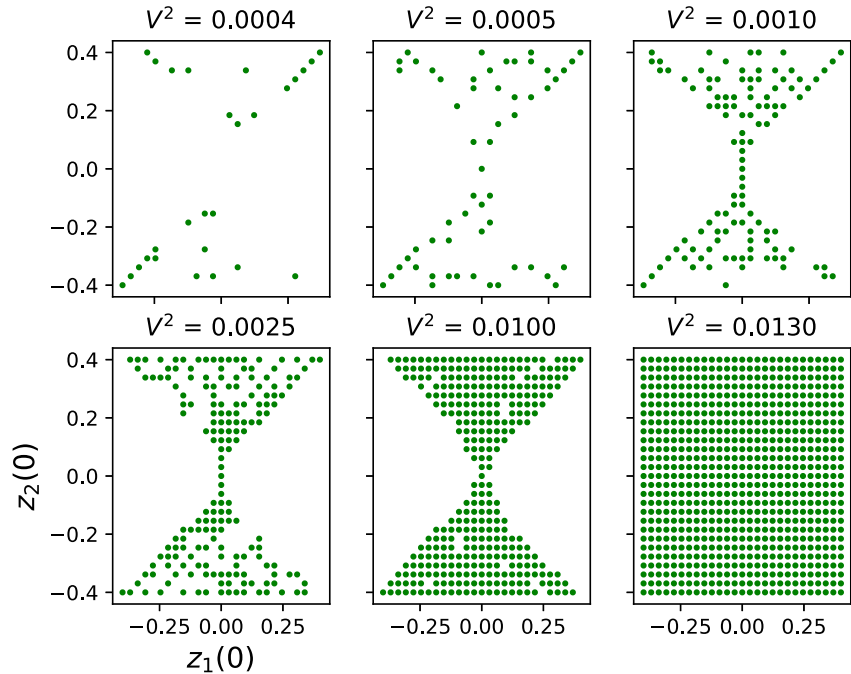


Fig. 7. Locking of LCOs for varying initial conditions and for coupling strengths near the threshold for locking. In this example $\sqrt{\kappa} = 0.90$. The x and y axes of each subplot are the initial conditions, $z_1(0)$ and $z_2(0)$. A point is plotted if the LCOs lock.

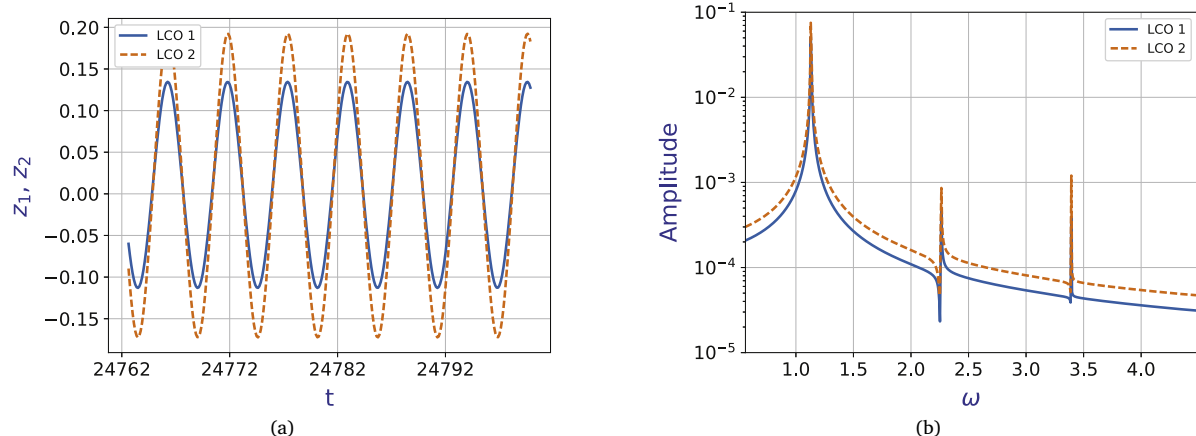


Fig. 8. Example of a case where LCOs lock. Results for $V^2 = 0.010$, $\sqrt{\kappa} = 0.90$, $z_2(0) = 0.25$, $z_1(0) = 0.266759$ (a) $z_1(t)$ and $z_2(t)$. (b) FFT of both signals.

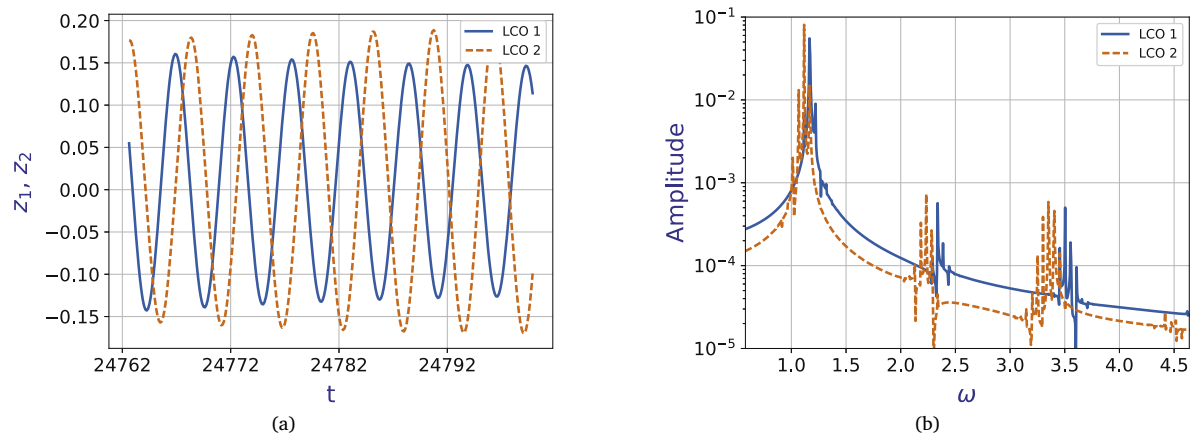


Fig. 9. Example of a case where LCOs drift. Results for $V^2 = 0.010$, $\sqrt{\kappa} = 0.90$, $z_2(0) = 0.25$, $z_1(0) = 0.266760$ (a) $z_1(t)$ and $z_2(t)$. (b) FFT of both signals.

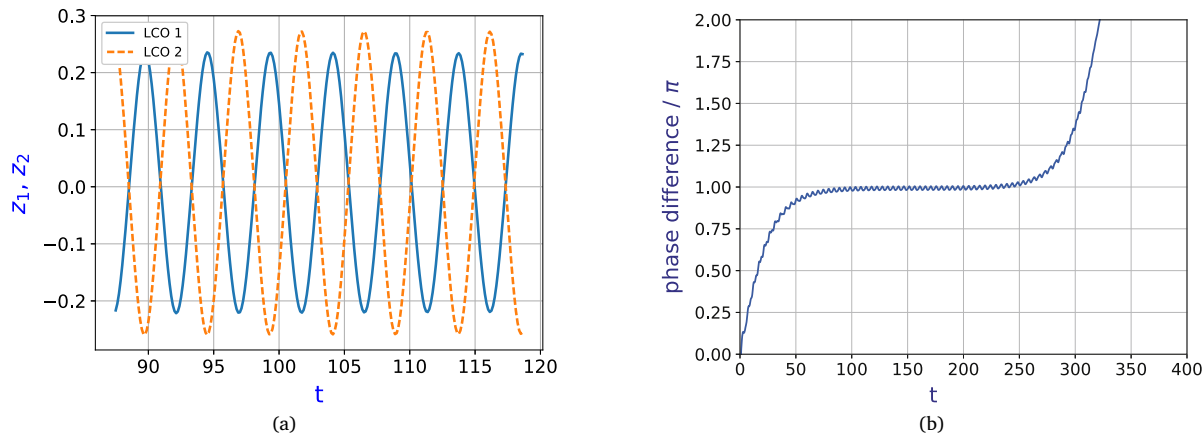


Fig. 10. Short time results for $V^2 = 0.010$, detuning ratio $\sqrt{\kappa} = 0.90$, $z_2(0) = 0.25$, $z_1(0) = 0.266760$ (a) $z_1(t)$ and $z_2(t)$ near the start of integration. (b) Difference in phase of LCO 1 and LCO 2 for short times.

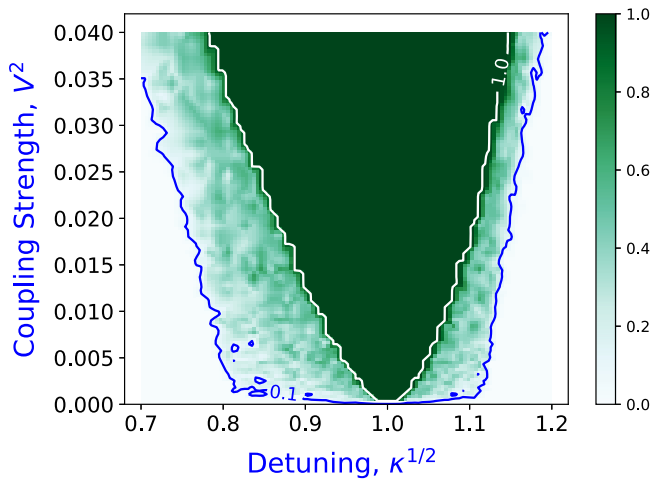


Fig. 11. Fraction of initial conditions, $z_1(0), z_2(0)$, holding all other I.C. to zero, that result in 1:1 locking as a function of the detuning ratio, $\sqrt{\kappa}$ and the coupling strength, V^2 .

van der Pol-Duffing and van der Pol–Mathieu oscillators 2:1 [47], 3:1 and 4:1 [19] locking were found. 3:1 locking of coupled tuning fork oscillators was experimentally observed in Ref. [21]. 3:1 locking of coupled modes was demonstrated in a Si disk resonator [48].

To test if the current system will support other than 1:1 locking the system of equations is modified to model beams with widely different frequencies. The original system, Eq. (3) is only intended to model beams with small levels of detuning. A simple modification is to allow the cubic stiffness of z_2 , as well as the linear stiffness, to scale with κ :

$$\ddot{z}_2 + \frac{\dot{z}_2}{Q} + \kappa(1 + CT_2)z_2 + \kappa\beta z_2^3 + \frac{V^2(z_2 - z_1)}{1 + |z_2 - z_1|^p} = DT_2 \quad (5)$$

Note that in an actual device the linear and cubic stiffnesses as well as other system will depend on the dimensions of the beam, and will not necessarily scale proportionally to each other.

Based on prior results, [46] we expect to be able to find regions of 2:1, 3:1 and higher integer ratio locking. Regions of locking at higher integer ratios may be indiscernible, but to confirm that at least some exist we also look for 3:2 and 5:2 locking. To discover and map the presence of these integer ratio locking regions, a sets of calculations was performed sweeping over $\sqrt{\kappa}$ and V^2 . Each integration starts at zero initial conditions and is continued until steady state oscillations are reached. Taking N:M to be 2:1, 3:1, 3:2 and 5:2 the oscillators are

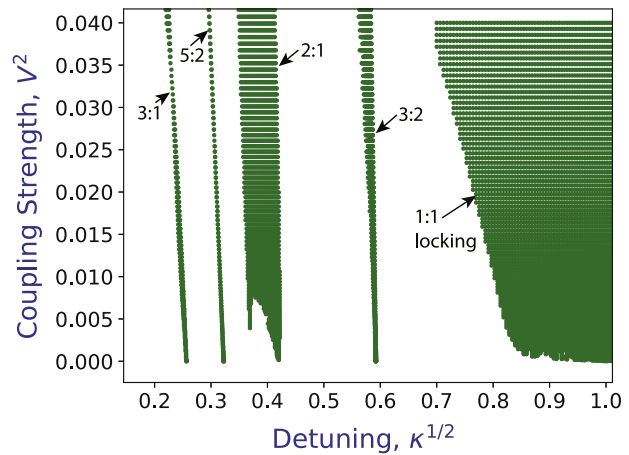


Fig. 12. Left half of 1:1 locking region using Eqs. (1)–(4). 2:1, 3:1, 3:2 and 5:2 locking regions using Eq. (5) to model LCO 2. Initial conditions are $z_1(0) = z_2(0) = 0$. At $V^2 = 0.04$, the 2:1 locking range spans uncoupled frequencies of $2.027 < \omega_1/\omega_2 < 2.333$. At $V^2 = 0.04$, the 3:1 locking range spans uncoupled frequencies of $3.317 < \omega_1/\omega_2 < 3.274$.

considered to be locked if $|\omega_1 - \frac{N}{M}\omega_2| < 0.001$. Note that due to the strong cubic nonlinearity the frequency of LCO 2 does not scale linearly with $\sqrt{\kappa}$. For example, when uncoupled, $\omega_2 = \frac{1}{2}\omega_1$ corresponds to $\sqrt{\kappa} = 0.42$ rather than $\sqrt{\kappa} = 0.5$.

The results of these calculations are shown in Fig. 12. These results show, for zero initial conditions, the 2:1, 3:1, 3:2 and 5:2 lock regions, along with the left half of the 1:1 lock region. All of the higher integer ratio locking regions are much smaller than the 1:1 lock region. The 5:2 and 3:1 regions, in particular, are very narrow. In all cases the lock regions tilt toward lower $\sqrt{\kappa}$ values as V^2 increases. This corresponds to higher unlocked $\omega_1 : \omega_2$ ratios as V^2 increases. Note that similar to the 1:1 lock results, the 2:1 lock region shows erosion of the lower boundary. Also similar to the 1:1 locking, for low values of coupling the lock region boundaries were found to be sensitive to initial conditions. Locking at other integer ratios is likely but is not explored here.

To gain a better understanding of the results consider a specific case: At $\sqrt{\kappa} = 0.413$ the uncoupled frequencies are $\omega_1 = 1.173$ and $\omega_2 = 0.579$, with a 2.027:1 ratio. When coupled and locked the frequencies are $\omega_1 = 1.202$ and $\omega_2 = 0.601$, a 2:1 ratio. Note that the coupling increases the frequencies of both oscillators, unlike the 1:1 locking in which the lock frequency is approximately equal to the uncoupled frequency of the slower oscillator, see Fig. 5.

For $V^2 = 0.04$ the 2:1 lock region spans $0.350 < \sqrt{\kappa} < 0.413$ corresponding to a span of uncoupled frequency ratios from 2.333:1 to 2.027:1. For $V^2 = 0.04$ the 3:1 lock region spans $0.222 < \sqrt{\kappa} < 0.226$ corresponding to a span of uncoupled frequency ratios from 3.317:1 to 3.274:1.

7. Summary and conclusions

A sixth order model of two coupled limit cycles oscillators is studied here. The model is motivated by the physical problem of the electrostatic coupling of a pair of doubly clamped microbeams, set into limit cycle oscillation by laser illumination and coupled due to an imposed difference in electrostatic voltage between the beams.

- Using system parameters approximated from experiments [36, 37, 24, 49, 35] the models show that even with low levels of coupling, pairs of microbeams can weakly lock at to each other at 1:1 frequency ratio over a relatively large range of detunings, approximately $\pm 10\%$ in linear frequency (Fig. 6(b)). In prior experiments [35] on single oscillators, frequencies in the range of 1 MHz were observed, thus the analysis here would suggest that for those devices, locking over a range of ± 100 kHz may be observable.
- The width of the 1:1 lock region is reduced if the strength of the cubic stiffness nonlinearity is reduced.
- Locking at 2:1, 3:1 3:2, and 5:2 frequency ratios is observed. Of these, the 2:1 locking region is the widest and likely the most accessible in actual devices.
- At the lowest levels of coupling lock and drift modes exist simultaneously, separated in the space of initial conditions.
- For weak coupling a fraction of initial conditions will lead to locking. As the coupling strength is increased, or the detuning decreased, all initial conditions will lead to locking.

Future work will consider the dynamics of an array of oscillators with systematically varying linear frequencies. Questions to be addressed would be: Do blocks of oscillators lock to each other? How does the number of oscillators and the associated frequency span of the blocks vary with coupling strength [50]?

Acknowledgments

This material is based upon work supported by the National Science Foundation under grant number CMMI-1634664. The third author acknowledges support from the Henry and Dinah Krongold Chair of Microelectronics and the Mary Shepard B. Upson Visiting Professorship in Engineering, Cornell University. Computations were performed through the Extreme Science and Engineering Discovery Environment (XSEDE), which is supported by National Science Foundation, grant number ACI-1548562. This work used the XSEDE resources Stampede 2 at the Texas Advanced Computing Center (TACC) and Bridges at the Pittsburgh Supercomputing Center (PSC) through allocations TG-MSS160022 and TG-MSS170032.

References

- [1] C.-F. Chiang, A.B. Graham, B.J. Lee, C.H. Ahn, E.J. Ng, G.J. O'Brien, T.W. Kenny, Resonant pressure sensor with on-chip temperature and strain sensors for error correction, in: IEEE 26th International Conference on Micro Electro Mechanical Systems, MEMS, IEEE, 2013, pp. 45–48.
- [2] J.D. Zook, W.R. Herb, C.J. Bassett, T. Stark, J.N. Schoess, M.L. Wilson, Fiber-optic vibration sensor based on frequency modulation of light-excited oscillators, Sensors Actuators A 83 (2000) 270–276.
- [3] B. Ilic, D. Czaplewski, H.G. Craighead, P. Neuzil, C. Campagnolo, C. Batt, Mechanical resonant immunospecific biological detector, Appl. Phys. Lett. 77 (2000) 450–452.
- [4] D.E. Serrano, F. Ayazi, MEMS inertial sensors, in: Resonant MEMS: Fundamentals, Implementation, and Application, John Wiley & Sons, 2015, pp. 329–354.
- [5] P. Zwahlen, Y. Dong, A.-M. Nguyen, F. Rudolf, J.-M. Stauffer, P. Ullah, V. Ragot, Breakthrough in high performance inertial navigation grade sigma-delta MEMS accelerometer, in: Position Location and Navigation Symposium, PLANS, 2012 IEEE/ION, IEEE, 2012, pp. 15–19.
- [6] D. Peroulis, S. Pacheco, K. Sarabandi, L.P. Katehi, Tunable lumped components with applications to reconfigurable MEMS filters, in: Microwave Symposium Digest, 2001 IEEE MTT-S International, vol. 1, IEEE, 2001, pp. 341–344.
- [7] R.H. Olsson III, J.G. Fleming, K.E. Wojciechowski, M.S. Baker, M.R. Tuck, Post-CMOS compatible aluminum nitride MEMS filters and resonant sensors, in: Frequency Control Symposium, 2007 Joint with the 21st European Frequency and Time Forum, IEEE International, IEEE, 2007, pp. 412–419.
- [8] A.L. Brady, M.M. McDonald, S.N. Theriault, B. Smith, The impact of silicon MEMS on the future of ink jet printhead design and performance, in: International Conference on Digital Printing Technologies, 2005, pp. 264–267.
- [9] R. Ryf, D.T. Neilson, V.A. Aksyuk, Optical switching, Elsevier, 2006, pp. 169–213 ch. MEMS based optical switching.
- [10] O. Brand, I. Dufour, S. Heinrich, F. Josse, Resonant MEMS: Fundamentals, Implementation, and Application, John Wiley & Sons, 2015.
- [11] M.I. Younis, MEMS Linear and Nonlinear Statics and Dynamics, Springer Science & Business Media, 2011.
- [12] K. Ekinci, M. Roukes, Nanoelectromechanical systems, Rev. Sci. Instrum. 76 (6) (2005) 061101.
- [13] W.J. Venstra, M.J. Capener, S.R. Elliott, Nanomechanical gas sensing with nonlinear resonant cantilevers, Nanotechnology 25 (42) (2014) 425501.
- [14] Y. Linzon, B. Ilic, S. Lulinsky, S. Krylov, Efficient parametric excitation of silicon-on-insulator microcantilever beams by fringing electrostatic fields, J. Appl. Phys. 113 (16) (2013) 163508.
- [15] D.W. Storti, P.G. Reinhardt, Stability of in-phase and out-of-phase modes for a pair of linearly coupled van der Pol oscillators, in: A. Guran (Ed.), Nonlinear Dynamics, World Scientific, 1995, pp. 1–23.
- [16] D. Storti, P. Reinhardt, Phase-locked mode stability for coupled van der Pol oscillators, Trans. ASME. J. Vib. Acoust. 122 (3) (2000) 318–323.
- [17] T. Chakraborty, R. Rand, The transition from phase locking to drift in a system of two weakly coupled van der Pol oscillators, Int. J. Non-Linear Mech. 23 (5–6) (1988) 369–376.
- [18] D. Storti, R. Rand, Dynamics of two strongly coupled van der Pol oscillators, Int. J. Non-Linear Mech. 17 (3) (1982) 143–152.
- [19] M. Belhaq, A. Fahsi, Frequency-locking in nonlinear forced oscillators near 3:1 and 4:1 resonances, Ann. Solid Struct. Mech. 4 (1–2) (2012) 15–23.
- [20] M.H. Matheny, M. Grau, L.G. Villanueva, R.B. Karabalin, M. Cross, M.L. Roukes, Phase synchronization of two anharmonic nanomechanical oscillators, Phys. Rev. Lett. 112 (1) (2014).
- [21] D. Pu, X. Wei, L. Xu, Z. Jiang, R. Huan, Synchronization of electrically coupled micromechanical oscillators with a frequency ratio of 3:1, Appl. Phys. Lett. 112 (1) (2018) 013503.
- [22] S.H. Strogatz, R.E. Mirollo, Synchronization of pulse-coupled biological oscillators, SIAM J. Appl. Math. 50 (6) (1990) 1645–1662.
- [23] M. Pandey, K. Aubin, M. Zalalutdinov, R.B. Reichenbach, A.T. Zehnder, R.H. Rand, H.G. Craighead, Analysis of frequency locking in optically driven MEMS resonators, J. Microelectromech. Syst. 15 (6) (2006) 1546–1554.
- [24] D.B. Blocher, A.T. Zehnder, R.H. Rand, Entrainment of micromechanical limit cycle oscillators in the presence of frequency instability, J. Microelectromech. Syst. 22 (4) (2013) 835–845.
- [25] M.J. Seitner, M. Abdi, A. Ridolfo, M.J. Hartmann, E.M. Weig, Parametric oscillation, frequency mixing, and injection locking of strongly coupled nanomechanical resonator modes, Phys. Rev. Lett. 118 (25) (2017).
- [26] R. Adler, A study of locking phenomena in oscillators, Proc. IEEE 61 (10) (1973) 1380–1385.
- [27] R. Forke, D. Scheibner, J.E. Mehner, T. Gessner, W. Dotzel, Electrostatic force coupling of MEMS oscillators for spectral vibration measurements, Sensors Actuators A 142 (1) (2008) 276–283.
- [28] R. Forke, D. Scheibner, W. Dotzel, J. Mehner, Measurement unit for tunable low frequency vibration detection with MEMS force coupled oscillators, Sensors Actuators A 156 (1) (2009) 59–65.
- [29] S.Z. Lulec, U. Adiyam, G.G. Yaralioglu, Y. Leblebici, H. Urey, MEMS cantilever sensor array oscillators: Theory and experiments, Sensors Actuators A 237 (2016) 147–154.
- [30] M.-H. Li, C.-Y. Chen, W.-C. Chen, S.-S. Li, A vertically coupled MEMS resonator pair for oscillator applications, J. Microelectromech. Syst. 24 (3) (2015) 528–530.
- [31] D.K. Agrawal, J. Woodhouse, A.A. Seshia, Synchronization in a coupled architecture of microelectromechanical oscillators, J. Appl. Phys. 115 (16) (2014).
- [32] T. Sahai, A.T. Zehnder, Modeling of coupled dome-shaped microoscillators, J. Microelectromech. Syst. 17 (3) (2008) 777–786.
- [33] D.K. Agrawal, J. Woodhouse, A.A. Seshia, Observation of locked phase dynamics and enhanced frequency stability in synchronized micromechanical oscillators, Phys. Rev. Lett. 111 (8) (2013) 084101.
- [34] K.L. Aubin, M.K. Zalalutdinov, T. Alan, R.B. Reichenbach, R.H. Rand, A.T. Zehnder, J.M. Parpia, H.G. Craighead, Limit cycle oscillations in CW laser-driven NEMS, J. Microelectromech. Syst. 13 (6) (2004) 1018–1026.
- [35] D.B. Blocher, Optically Driven Limit Cycle Oscillations in MEMS (Ph.D. thesis), Cornell University, 2012.

[36] D. Blocher, R.H. Rand, A.T. Zehnder, Analysis of laser power threshold for self oscillation in thermo-optically excited doubly supported MEMS beams, *Int. J. Non-Linear Mech.* 57 (2013) 10–15.

[37] D. Blocher, R.H. Rand, A.T. Zehnder, Multiple limit cycles in laser interference transduced resonators, *Int. J. Non-Linear Mech.* 52 (2013) 119–126.

[38] S. Krylov, N. Molinazzi, T. Shmilovich, U. Pomerantz, S. Lulinsky, Parametric excitation of flexural vibrations of micro beams by fringing electrostatic fields, in: Proceedings of the ASME Design Engineering Technical Conference IDET2010, vol. 4, 2010, pp. 601–611.

[39] S.Y. Linzon, B. Ilic, S. Krylov, Efficient parametric excitation of silicon-on-insulator microcantilever beams by fringing electrostatic field, *J. Appl. Phys.* 113 (2013) 163508.

[40] L. Petzold, A. Hindmarsh, LSODA, tech. rep., Computing and Mathematics Research Division, I-316 Lawrence Livermore National Laboratory, Livermore, CA 94550, 1997.

[41] A.V. Oppenheim, R.W. Schafer, J.R. Buck, *Discrete-Time Signal Processing*, third ed., Pearson, 2010.

[42] R.H. Rand, Lecture Notes on Nonlinear Vibrations, 2012. <http://hdl.handle.net/1813/28989>.

[43] Y. Wu, Z. Song, W. Liu, J. Jia, J. Xiao, Experimental and numerical study on the basin stability of the coupled metronomes, *Eur. Phys. J. Spec. Top.* 223 (4) (2014) 697–705.

[44] A.L. Fradkov, B. Andrievsky, Synchronization and phase relations in the motion of two-pendulum system, *Int. J. Non-Linear Mech.* 42 (6) (2007) 895–901.

[45] D.A. Wiley, S.H. Strogatz, M. Girvan, The size of the sync basin, *Chaos* 16 (1) (2006) 015103.

[46] W. Keith, R. Rand, 1:1 and 2:1 phase entrainment in a system of two coupled limit cycle oscillators, *J. Math. Biol.* 20 (2) (1984) 133–152.

[47] M. Belhaq, A. Fahsi, 2:1 and 1:1 frequency-locking in fast excited van der Pol Mathieu Duffing oscillator, *Nonlinear Dynam.* 53 (1–2) (2008) 139–152.

[48] P. Taheri-Tehrani, A. Guerrieri, M. Defoort, A. Frangi, D.A. Horsley, Mutual 3:1 subharmonic synchronization in a micromachined silicon disk resonator, *Appl. Phys. Lett.* 111 (18) (2017) 183505.

[49] D. Blocher, A.T. Zehnder, R.H. Rand, S. Mukerji, Anchor deformations drive limit cycle oscillations in interferometrically transduced MEMS beams, *Finite Elem. Anal. Des.* 49 (1) (2012) 52–57.

[50] N. Dick, S. Grutzik, C. Wallin, B.R. Ilic, S. Krylov, A.T. Zehnder, Actuation of higher harmonics in large arrays of micromechanical cantilevers for expanded resonant peak separation, *ASME. J. Vib. Acoust.* (2018) in press.